Flexural Frequency Analysis of Damaged Beams Using Mixture Unified Gradient Elasticity Theory+

Hossein Darban *[1], S. Ali Faghidian *[2]

[1] *Institute of Fundamental Technological Research, Polish Academy of Sciences, Pawińskiego 5B, 02-106 Warsaw, Poland*

[2] *Department of Mechanical Engineering, Science and Research Branch, Islamic Azad University, Tehran, Iran*

Abstract

The free transverse vibration of miniaturized beams with multiple edge cracks is investigated using the mixture unified gradient elasticity theory. The model captures both possible stiffening and softening size-dependent behaviors at small scales. The problem is addressed using the Bernoulli-Euler beam theory, with the domain partitioned into distinct sections at the locations of cracked cross-sections. To account for the discontinuities in bending slope and deflection, rotational and translational springs are introduced at these cracked cross-sections. The time-dependent variational functional associated with the mixture unified gradient elasticity theory is rigorously established to derive variationally consistent and extra non-standard boundary and continuity conditions. Natural frequencies are obtained by solving the eigenvalue problem resulting from the imposition of boundary and continuity conditions. The model predictions demonstrate excellent agreement with experimental data from the literature for large-scale beams. Furthermore, as the crack length tends to zero, the results converge with those of crack-free mixture unified gradient elastic beams reported in prior studies. The model is applied to examine the

* Corresponding authors: Hossein Darban (hdarban@ippt.pan.pl) ; S. Ali Faghidian (faghidian@srbiau.ac.ir; faghidian@gmail.com)

+ Preprint released under CC BY 4.0 licence. Published in Composite Structures Volume 363, 1 July 2025, 119143. DOI: https://doi.org/10.1016/j.compstruct.2025.119143

effects of gradient characteristic parameters, crack length and location, and boundary conditions on the frequencies. Novel findings and discussions presented here hold significance for the design, condition monitoring, and maintenance of miniaturized structures.

Keywords: Micro- and nanobeam; Frequency shift; Edge crack; Gradient elasticity; Resonator.

1. Introduction

Nowadays, cutting-edge technologies require devices to be as small as possible while consuming minimal energy and having the capability of being self-powered. These compact, cost-effective devices exhibit remarkable versatility and function effectively under diverse, sometimes challenging operational conditions. Micro- and nano-scale beams are crucial components in sensors and actuators, which are fundamental to micro- and nano-electromechanical systems (MEMS and NEMS). MEMS and NEMS resonators find widespread applications in various fields, including sensing and biomechanics [1]. Ensuring the reliability and functionality of micro- and nanobeams throughout their operational lifespan is paramount. However, they are prone to cracking due to manufacturing flaws, in-service loads, and environmental factors. Hence, understanding the mechanical behavior of cracked micro- and nanobeams is essential for advancing MEMS and NEMS technology. Moreover, this understanding is essential for (i) monitoring and maintaining micro- and nano-devices by detecting cracks using methods such as frequency shift measurements, and (ii) fostering innovative designs by intentionally introducing multiple cracks into these devices to manipulate their mechanical responses and achieve specific frequencies. Therefore, the present article aims to investigate the free transverse vibration of miniaturized cracked beams.

Several experimental studies have shown that the mechanical behavior of small-scale structures varies with size [2, 3]. As a result, applying structural theories based on the classical continuum mechanics to structures at small scales becomes inadequate. While atomistic methods can capture size effects accurately, their extensive computational requirements limit their practicality. Non-classical continuum

mechanics-based theories, such as couple stress theory, micropolar theory, surface elasticity theory, fractional calculus-based theories, modified couple stress theory, strain gradient theory, modified strain gradient theory, and nonlocal elasticity theories, offer a feasible compromise between accuracy and computational efficiency. Many models based on these non-classical continuum mechanics-based theories have been developed in the literature to investigate the size-dependent mechanical behavior of both crack-free and cracked structures at small scales [4–18].

Based on the available experimental results in the literature, the behavior of materials at small scales may vary. More precisely, while some researchers reported a stiffer response as the dimension of structures reduced [2, 3], some studies reported that normalized bending stiffness of micro- and nanobeams could remain constant [19] or even decrease with decreasing dimensions [20, 21]. Therefore, it is of utmost importance for a non-classical model to be able to capture both possible stiffening and softening responses of structures at the small scales. However, this is not the case for the Eringen nonlocal and strain gradient theories. While theories rooted in the strain gradient theory of elasticity primarily account for the stiffening behavior (e.g. [22]), those based on Eringen's nonlocal integral elasticity theory predict only a softening behavior in structures at small scales. Thus, there is a growing interest in merging concepts from various non-classical continuum mechanics-based theories to enhance their scope of application. One such outcome of this endeavor is the nonlocal strain gradient theory [23], which combines nonlocal elasticity and strain gradient theory. A more recent development is the introduction of the mixture unified gradient theory of elasticity [24]. This theory integrates elements from the stress gradient model, strain gradient model, and classical elasticity theory, enabling it to effectively capture both stiffening and softening behaviors in small-scale structures. The mixture unified gradient theory has been successfully applied to address size effect phenomena in various structural problems [24–26].

The mixture unified gradient theory of elasticity was originally formulated for micro- and nanobeams featuring continuous field variables [24]. The model was further developed in [27] to address nanobeams subjected to a concentrated load along their span, leading to the derivation of a set of non-standard

interface conditions. Following [27] and given the potential of the mixture unified gradient theory to address size-dependent mechanical responses in small-scale structures by capturing both stiffening and softening effects, this theory is extended herein to accommodate scenarios where the beam contains multiple edge cracks. In such instances, the beam domain needs to be partitioned into distinct sections, and appropriate boundary and continuity conditions must be imposed. To achieve this, the time-dependent functional associated with the mixture unified gradient theory of elasticity is decomposed at the cracked cross-sections, and extra non-standard boundary and continuity conditions are derived through rigorous mathematical procedures. These non-standard conditions, combined with the standard variationally consistent boundary and continuity conditions, are then applied to calculate the natural frequencies of small-scale beams with multiple edge cracks.

The article is structured as follows. Section 2 outlines the problem definition and formulation, along with discussions on kinematic assumptions. Particularly, continuity conditions at cracked cross-sections are established by introducing rotational and translational springs. Consequently, the bending slope and deflection exhibit jumps at cracked cross-sections, proportional to the bending moment and shear force transmitted through the cross-section. In the Section 3, the formulated model is applied to small-scale beams with one and two cracks. Frequencies, up to the fourth mode of vibrations, are presented for beams under different boundary conditions and characteristic parameters. Finally, Section 4 presents the conclusions drawn from the study.

2. Problem Definition and Formulation

Consider the free transverse vibration of the small-scale slender beam depicted in Fig. 1(a). Cartesian coordinate system *x*-*z* is established at the centroidal axis of the beam and its left end. Without loss of generality, it is assumed that the beam features a rectangular cross-section $h \times b$, and has n edge cracks with lengths a_i at specific locations denoted as x_i for $i = 1 \ldots, n$. The small-scale beam is composed of an isotropic homogeneous material with Young's modulus E. The flexural stiffness and length of the

beam are defined by, respectively, $EI = Ebh^3/12$ and L. The presence of n cracks partitions the beam into $n + 1$ sections. Both cracks and sections are numbered from left to right. Here and throughout the derivation, ${}^{(j)}F$ and F_i define the quantity F associated with, respectively, the section j and the cracked cross-section i. Moreover, the m-th derivative of the quantity F with respect to x is denoted by $F_{,\underbrace{xxxx...x}_{m \text{ times}}}$.

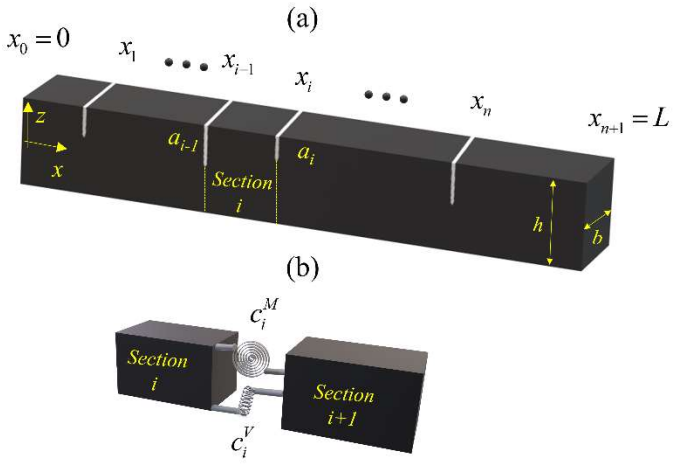

Fig. 1 (a) Small-scale beam with n cracks. (b) Rotational and translational springs used to model the effect of the crack.

2.1. Kinematic Assumptions

Since the considered small-scale beam is slender, shear deformations are neglected [28], and the displacement field is described using the Bernoulli-Euler beam model:

$$ {}^{(i)}u_x = -z\,{}^{(i)}v_{,x}(x), \qquad {}^{(i)}u_z = {}^{(i)}v(x) \tag{1} $$

where ${}^{(i)}u_x$ and ${}^{(i)}u_z$ are, respectively, the axial and transverse displacements of section i. The first derivative of the transverse displacement, ${}^{(i)}v_{,x}$, denotes the bending slope.

The free transverse vibration of a cracked beam presents a complex nonlinear problem due to the periodic opening and closing of the crack faces, known as the breathing phenomenon. Consequently, formulating

the problem analytically proves challenging. The aforementioned nonlinearity is addressed in Ref. [29] by modeling it as a piecewise linear system. This approach enables the approximation of the natural frequencies of a cracked beam by integrating the two extreme solutions obtained under the assumption of either the crack always being open or always being closed. For the sake of obtaining analytical solutions to the problem of a cracked beam, it is commonly assumed that the crack remains open throughout the vibration [6, 30]. The same assumption is, thus, adopted in this study.

Assuming that the cracks are always open, the transverse displacement and the bending slope exhibit discontinuities at the cracked cross-sections due to the local flexibilities of the cracks. In structural analysis, these discontinuities are typically modeled by introducing elastic rotational and translational springs at the cracked cross-sections [6, 16, 31], as illustrated in Fig. 1(b). Therefore, the kinematic continuity conditions at the cracked cross-section located at $x = x_i$ are:

$$\begin{aligned} {}^{(i+1)}v_{,x}\left(x_i\right) - {}^{(i)}v_{,x}\left(x_i\right) &= c_i^M \;\; {}^{(i)}M\left(x_i\right) \\ {}^{(i+1)}v\left(x_i\right) - {}^{(i)}v\left(x_i\right) &= c_i^V \;\; {}^{(i)}V\left(x_i\right) \end{aligned} \tag{2}$$

for $i = 1, \ldots, n$. The quantities ${}^{(i)}M\left(x_i\right)$ and ${}^{(i)}V\left(x_i\right)$ are, respectively, the bending moment and the shear force acting on the cracked cross-section. The parameters c_i^M and c_i^V denote the compliances of the i-th crack, which can correspond, respectively, to the mode I and mode II stress intensity factors induced by the bending moment and the shear force. Closed-form expressions of the crack compliances in terms of the crack length are provided in Appendix A for a rectangular beam with an edge crack under plane-stress conditions.

2.2. Governing Equations

The time-dependent variational functional $\mathbb{P}$ consistent with the Bernoulli-Euler beam model within the framework of the mixture unified gradient theory reads [25]:

$$\mathbb{P}=\int_0^L\Bigg(M_0\left(x,t\right)v_{,xx}\left(x,t\right)+\frac{1}{2EI}\left(M_0\left(x,t\right)\right)^2+\frac{c^2}{2EI}\left(M_{0,x}\left(x,t\right)\right)^2+M_1\left(x,t\right)v_{,xxx}\left(x,t\right)$$
$$+\frac{1}{2EI\left(\alpha c^2+\ell^2\right)}\left(M_1\left(x,t\right)\right)^2+\frac{c^2}{2EI\left(\alpha c^2+\ell^2\right)}\left(M_{1,x}\left(x,t\right)\right)^2\Bigg)dx \tag{3}$$

as the time is denoted by *t*. The resultant moments M_0 and M_1 are defined as the dual fields of the flexural curvature $\chi=v_{,xx}$ and its first-order derivative along the *x*-axis $\chi_{,x}=v_{,xxx}$, respectively. Introductions of (i) the stress gradient characteristic length c, (ii) the strain gradient length-scale parameter ℓ, and (iii) the mixture parameter α address the significance of the corresponding gradient theory of elasticity. More precisely, incorporating these gradient and mixture parameters, the mixture unified gradient theory can capture both stiffening and softening effects at small scales. These parameters can be calibrated using the experimental or atomistic results.

Taking the first variation of the functional while treating the kinematic and kinetic field variables independently, and applying Green's theorem on the kinetic field variables, we arrive at:

$$\delta\mathbb{P}=\int_0^L\left(M_0\delta v_{,xx}+M_1\delta v_{,xxx}\right)dx+\frac{1}{EI}\int_0^L\left(M_0-c^2M_{0,xx}+EIv_{,xx}\right)\delta M_0dx+$$
$$\frac{1}{EI\left(\alpha c^2+\ell^2\right)}\int_0^L\left(M_1-c^2M_{1,xx}+EI\left(\alpha c^2+\ell^2\right)v_{,xxx}\right)\delta M_1dx+ \tag{4}$$
$$\frac{1}{EI}c^2\left(M_{0,x}\,\delta M_0\right)\Big|_0^L+\frac{1}{EI\left(\alpha c^2+\ell^2\right)}c^2\left(M_{1,x}\,\delta M_1\right)\Big|_0^L$$

The boundary terms can be released due to the heuristic assumption on the virtual kinetic test field variables to have compact support on the domain boundary [24]. Prescribing the stationarity of the

introduced time-dependent variational functional, the constitutive laws of the resultant moments M_0 and M_1, valid for each section of the cracked small-scale beam [25], are determined as:

$$\begin{aligned} {}^{(i)}M_0 - c^2\,{}^{(i)}M_{0,xx} &= -EI\,{}^{(i)}v_{,xx} \\ {}^{(i)}M_1 - c^2\,{}^{(i)}M_{1,xx} &= -EI\left(\alpha c^2 + \ell^2\right){}^{(i)}v_{,xxx} \end{aligned} \tag{5}$$

for $i = 1, \ldots, n+1$. Introducing the total bending moment ${}^{(i)}M$ as [24]:

$${}^{(i)}M = {}^{(i)}M_0 - {}^{(i)}M_{1,x} \tag{6}$$

the following equation can state both constitutive laws provided in Eq. (5) [25]:

$${}^{(i)}M - c^2\,{}^{(i)}M_{,xx} = -EI\left(v_{,xx} - \left(\alpha c^2 + \ell^2\right){}^{(i)}v_{,xxxx}\right) \tag{7}$$

Following [27], the governing equations and the consistent boundary and continuity conditions at the cracked cross-sections are, afterward, derived by prescribing the stationarity of the functional, $\delta\mathbb{P} = 0$:

$$\begin{aligned} \delta\mathbb{P} &= \int_0^L \left(M_0\delta v_{,xx} + M_1\delta v_{,xxx}\right)dx = \sum_{i=1}^{n+1}\int_{x_{i-1}}^{x_i} {}^{(i)}\left(M_0\delta v_{,xx} + M_1\delta v_{,xxx}\right)dx = \\ &\sum_{i=1}^{n+1}\int_{x_{i-1}}^{x_i} {}^{(i)}\left(M_{,xx}\,\delta v\right)dx + \sum_{i=1}^{n+1} {}^{(i)}\left(M\,\delta v_{,x} - M_{,x}\,\delta v\right)\Big|_{x_{i-1}}^{x_i} + \sum_{i=1}^{n+1} {}^{(i)}\left(M_1\delta v_{,xx}\right)\Big|_{x_{i-1}}^{x_i} \end{aligned} \tag{8}$$

Given the first term in the right-hand side of the equation, the equation of motion governing the free transverse vibration of the i-th section, for $i = 1, \ldots, n+1$, is derived by the application of the d'Alembert principle as follows [25]:

$${}^{(i)}M_{,xx} + I_2\,{}^{(i)}\ddot{v}_{,xx} - I_0\,{}^{(i)}\ddot{v} = 0 \tag{9}$$

with $(I_o, I_2) = \int_A \rho(1, z^2) dA = (m, mh^2/12)$, where m is the mass per unit length of the beam. The time derivatives are shown by dots over the transverse displacement. Notably, the equation of motion has the standard form of the Bernoulli-Euler beam model.

Substitution of ${}^{(i)}M_{,xx}$ from Eq. (9) into (7) yields the following closed-form expression for the bending moment [25]:

$$ {}^{(i)}M = -EI\left({}^{(i)}v_{,xx} - \left(\alpha c^2 + \ell^2\right){}^{(i)}v_{,xxxx}\right) + c^2\left(I_0\,{}^{(i)}\ddot{v} - I_2\,{}^{(i)}\ddot{v}_{,xx}\right) \tag{10} $$

The constitutive equation is of higher order than the one of the classical theory, which can be recovered from Eq. (10) by setting $c, \ell \to 0$.

An explicit expression can be obtained for ${}^{(i)}M_1$ by following straightforward mathematics [25]:

$$ {}^{(i)}M_1 = -\frac{\left(\alpha c^2 + \ell^2\right)c^4}{c^2(1-\alpha) - \ell^2}\left(-I_0\,{}^{(i)}\ddot{v}_{,x} + I_2\,{}^{(i)}\ddot{v}_{,xxx}\right) - EI\left(\alpha c^2 + \ell^2\right){}^{(i)}v_{,xxx} + EI\frac{\left(\alpha c^2 + \ell^2\right)c^2}{c^2(1-\alpha) - \ell^2}\,{}^{(i)}v_{,xxxxx} \tag{11} $$

The equation of motion in terms of the transverse displacement is derived by substituting the bending moment Eq. (10) into the governing equation of motion Eq. (9):

$$ EI\left(\alpha c^2 + \ell^2\right){}^{(i)}v_{,xxxxxx} - EI\,{}^{(i)}v_{,xxxx} + I_0 c^2\,{}^{(i)}\ddot{v}_{,xx} - I_2 c^2\,{}^{(i)}\ddot{v}_{,xxxx} + I_2\,{}^{(i)}\ddot{v}_{,xx} - I_0\,{}^{(i)}\ddot{v} = 0 \tag{12} $$

Using the standard method of the separation of variables and assuming the harmonic solution as ${}^{(i)}v(x,t) = {}^{(i)}\psi(x)e^{i\omega t}$, the characteristic equation, spatial equation of motion, for section *i* is derived as:

$$EI\left(\alpha c^2+\ell^2\right)^{(i)}\psi_{,xxxxxx}+\left(I_2c^2\omega^2-EI\right)^{(i)}\psi_{,xxxx}-\omega^2\left(I_0c^2+I_2\right)^{(i)}\psi_{,xx}+I_0\omega^{2\,(i)}\psi=0 \tag{13}$$

for $i = 1, \ldots, n + 1$. The derived dynamic equilibrium equation is a sixth-order differential equation, noticeably distinct from the classical fourth-order equation consistent with the Bernoulli-Euler beam theory. Along this school of thought, similar higher-order equations of motion have been derived in prior studies for the dynamics of small-scale rods and beams, each employing distinct approaches to address size effects. For instance, strain gradient theories developed in [32–34] for studying the size-dependent dynamics of small-scale mass sensors yielded higher-order equations compared to classical formulations. Analogous findings were observed in [35] when applying the stress-driven nonlocal theory to investigate the vibration of small-scale cracked beams.

The solution of the dynamic equilibrium equation for section i, Eq. (13), depends on six unknown integration constants. Therefore, when analyzing a small-scale beam with n cracks, the solutions to the governing equations are expressed in terms of $6(n+1)$ unknown constants. The corresponding eigenvalue problem is formulated by imposing $6(n+1)$ standard variational and extra non-standard boundary and continuity conditions. From which, $2(n+1)$ extra non-standard boundary and continuity conditions are derived by prescribing the stationary of the introduced functional, i.e. vanishing the last term on the right-hand side of Eq. (8):

$$\begin{aligned}
&{}^{(1)}M_1\left(x_0,t\right)={}^{(n+1)}M_1\left(x_{n+1},t\right)=0\\
&{}^{(i)}M_1\left(x_i,t\right)={}^{(i+1)}M_1\left(x_i,t\right)\\
&{}^{(i)}v_{,xx}\left(x_i,t\right)={}^{(i+1)}v_{,xx}\left(x_i,t\right)
\end{aligned} \tag{14}$$

for $i = 1, \ldots, n$. The non-standard boundary and continuity conditions presented above are consistent with those derived in [27]. The remaining conditions are the 4 variationally consistent boundary conditions at x_0 and x_{n+1}, $2n$ kinematic compatibility conditions at the cracked cross-sections provided in Eq. (2),

and $2n$ variationally consistent kinetic conditions on the continuity of the bending moment and shear force at the cracked cross-sections:

$$\begin{aligned} {}^{(i)}M\left(x_i,t\right) &= {}^{(i+1)}M\left(x_i,t\right) \\ {}^{(i)}M_{,x}\left(x_i,t\right) &= {}^{(i+1)}M_{,x}\left(x_i,t\right) \end{aligned} \tag{15}$$

for i = 1, …, n. All the above-mentioned $6\left(n+1\right)$ conditions can be solely stated in terms of the transverse displacements of the sections, ${}^{(i)}\psi\left(x\right)$, using the following equations for ${}^{(i)}M$ and ${}^{(i)}M_1$:

$${}^{(i)}M = \left[-EI\left({}^{(i)}\psi_{,xx} - \left(\alpha c^2+\ell^2\right){}^{(i)}\psi_{,xxxx}\right) - c^2\omega^2\left(I_0\,{}^{(i)}\psi - I_2\,{}^{(i)}\psi_{,xx}\right)\right]e^{i\omega t} \tag{16}$$

$${}^{(i)}M_1 = \left[\frac{\left(\alpha c^2+\ell^2\right)c^4}{c^2\left(1-\alpha\right)-\ell^2}\omega^2\left(-I_0\,{}^{(i)}\psi_{,x} + I_2\,{}^{(i)}\psi_{,xxx}\right) - EI\left(\alpha c^2+\ell^2\right){}^{(i)}\psi_{,xxx} + EI\,\frac{\left(\alpha c^2+\ell^2\right)c^2}{c^2\left(1-\alpha\right)-\ell^2}\,{}^{(i)}\psi_{,xxxxx}\right]e^{i\omega t} \tag{17}$$

The imposition of $6\left(n+1\right)$ conditions in terms of ${}^{(i)}\psi\left(x\right)$ yields a homogeneous system of algebraic equations, whose nontrivial solution exists only if the determinant of the coefficient matrix vanishes. The natural frequencies are, subsequently, determined by finding the roots of the determinant of the coefficient matrix. The bisection method is used to find the roots numerically.

Last but not least, the solution approach implemented in this study is formulated in terms of kinematic field variables. Meanwhile, alternative structural problems, featuring kinetic field variables, can be treated by applying a series solution form [36, 37]. Dissimilar solution methodologies have been proposed in the literature to seek every possibility for the structural characteristics of sophisticated problems.

3. Results and Discussions

The established size-dependent model is utilized in this section to investigate frequency shifts in small-scale beams with one or two cracks. The effects of various parameters, including stress and strain gradient characteristic lengths, the mixture parameter as well as crack length and location on the frequencies, are thoroughly examined up to the fourth mode of vibration. Four typical boundary conditions, namely, clamped-free, pinned-pinned, clamped-pinned, and clamped-clamped, are considered. The results are presented using the following dimensionless parameters:

$$\zeta = \frac{c}{L};\quad \eta = \frac{\ell}{L};\quad \bar{x} = \frac{x}{L};\quad \bar{h} = \frac{h}{L};\quad \bar{\omega} = \omega L^2\sqrt{m/EI} \tag{18}$$

3.1. Verification

Before presenting numerical results associated with the frequencies of mixture unified gradient elastic beams with cracks, the validity of the established size-dependent model is assessed by comparing its predictions for two limiting cases with available experimental and analytical solutions in the literature. The first case refers to experimental work on the frequencies of a large-scale cracked clamped-free beam as reported in [38]. Ratios between the first four frequencies of the cracked and crack-free beams predicted by the present model for $\zeta, \eta \to 0$, which reduces the model to a classical formulation, and the corresponding experimental results, are depicted in Fig. 2. The mixture parameter loses its effect on the results due to the vanishing gradient parameters. The geometrical characteristics of the beams are described in the illustration caption. The figure illustrates an excellent agreement between the predictions of the present model and the experimental results for the case of mesoscale cracked beams, even at higher modes of vibrations and longer cracks.

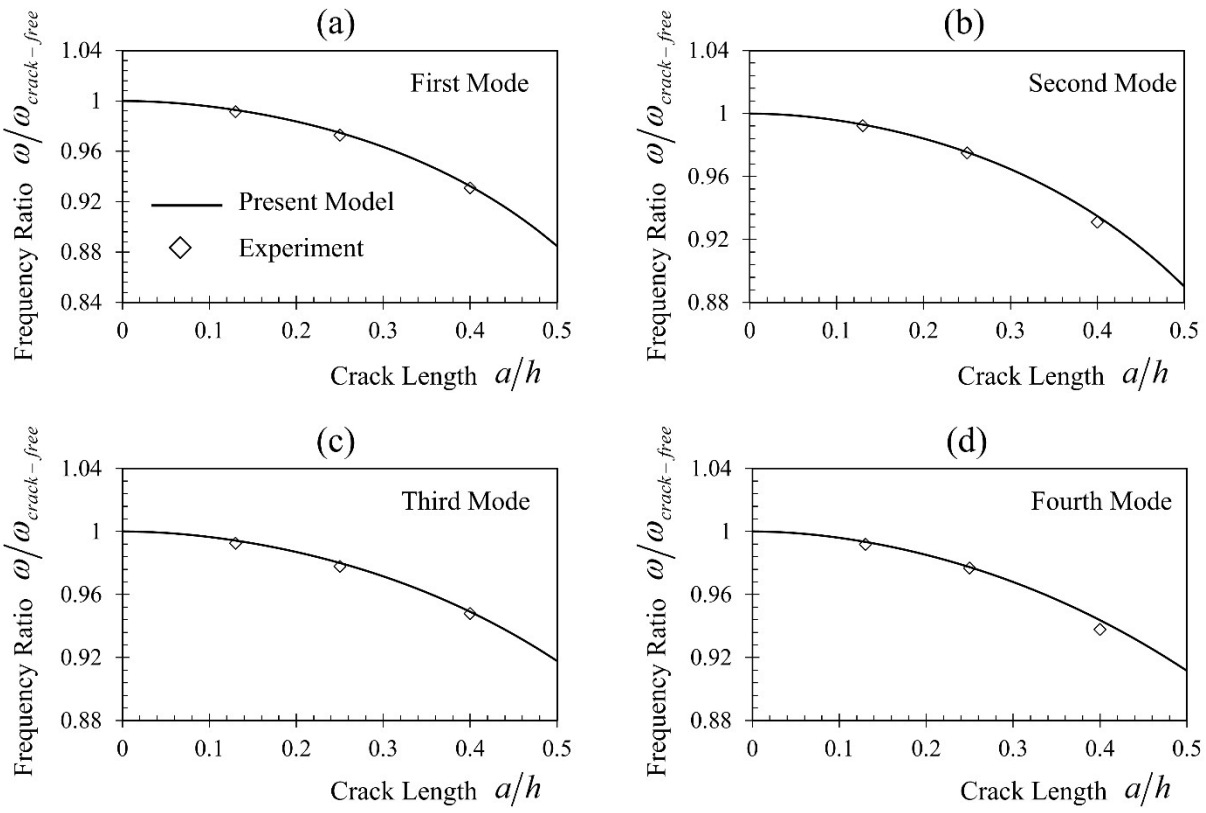

Fig. 2 Ratios between the (a) first, (b) second, (c) third, and (d) fourth natural frequencies of a cracked clamped-free beam with $\bar{h} = 0.039$ and those of a crack-free beam, as predicted by the present model for $\zeta, \eta \to 0$. The experimental data reported in [38] for mesoscale beams are also provided. The crack locations for the first to fourth modes of vibrations are 0.2, 0.55, 0.3, and 0.5, respectively.

The results of the second verification case are depicted in Fig. 3. Small-scale clamped-free and clamped-clamped beams with one crack located at the mid-span are considered, and the dimensionless fundamental natural frequencies are presented by decreasing the crack length from $a/h = 0.6$ to 0. The thickness-to-length ratio is $\bar{h} = 0.1732$, and the gradient and mixture parameters are chosen as $\zeta = 0.6$, and $\eta = \alpha = 0.5$. As anticipated, the natural frequencies are higher for beams with shorter cracks. When the crack length tends to zero, the predictions of the present model align with those reported in [25] for a crack-free mixture unified gradient elastic beam.

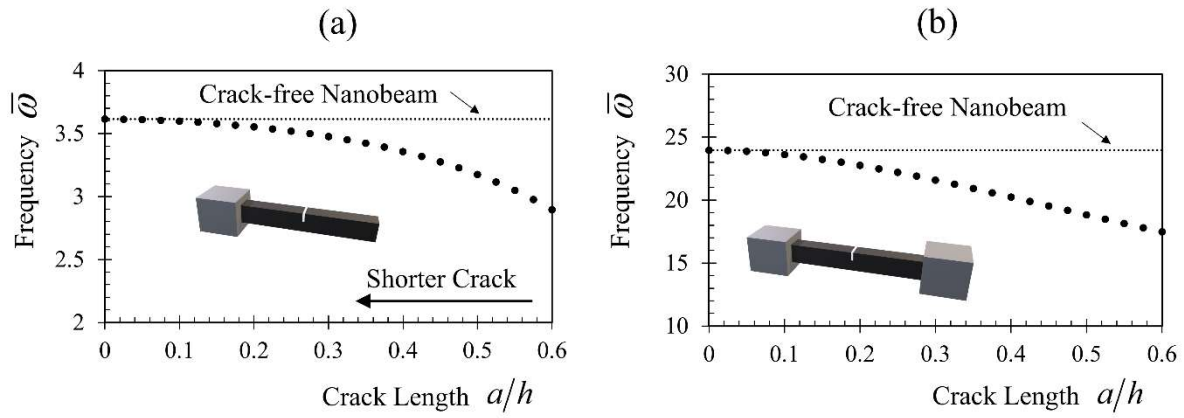

Fig. 3 Convergence of the fundamental natural frequencies predicted by the present model to the corresponding data in [25] for a crack-free small-scale beam on reducing the crack length to zero. The results are presented for the (a) clamped-free and (b) clamped-clamped small-scale beams with one crack at $\bar{x}_1 = 0.5$, $\bar{h} = 0.1732$, $\zeta = 0.6$, $\eta = \alpha = 0.5$.

3.2. One Crack

The fundamental natural frequencies are depicted in Fig. 4 for small-scale beams with various boundary conditions. Beams have a thickness-to-length ratio of $\bar{h} = 0.1$ and one crack with a length of $a/h = 0.5$, located at mid-span. The mixture parameter is fixed at 0.5, and the results are displayed for different stress and strain gradient parameters.

It has been observed in [25] that stress and strain gradient characteristic length parameters exhibit softening and stiffening effects, respectively, on the response of crack-free mixture unified gradient elastic beams. This behavior is similarly confirmed here for cracked beams when examining the results in Fig. 4. As depicted in Fig. 4, an increase in the stress gradient parameter (ζ) consistently decreases the natural frequency irrespective of the boundary conditions. Conversely, increasing the strain gradient parameter (η) consistently increases the natural frequency. The magnitude of the impact of gradient parameters on natural frequencies significantly varies with boundary conditions. For instance, when the strain gradient parameter increases from 0 to 0.9 in the absence of the stress gradient parameter, the

natural frequency rises by 19%, 6%, 119%, and 82% for clamped-free, pinned-pinned, clamped-pinned, and clamped-clamped small-scale beams, respectively.

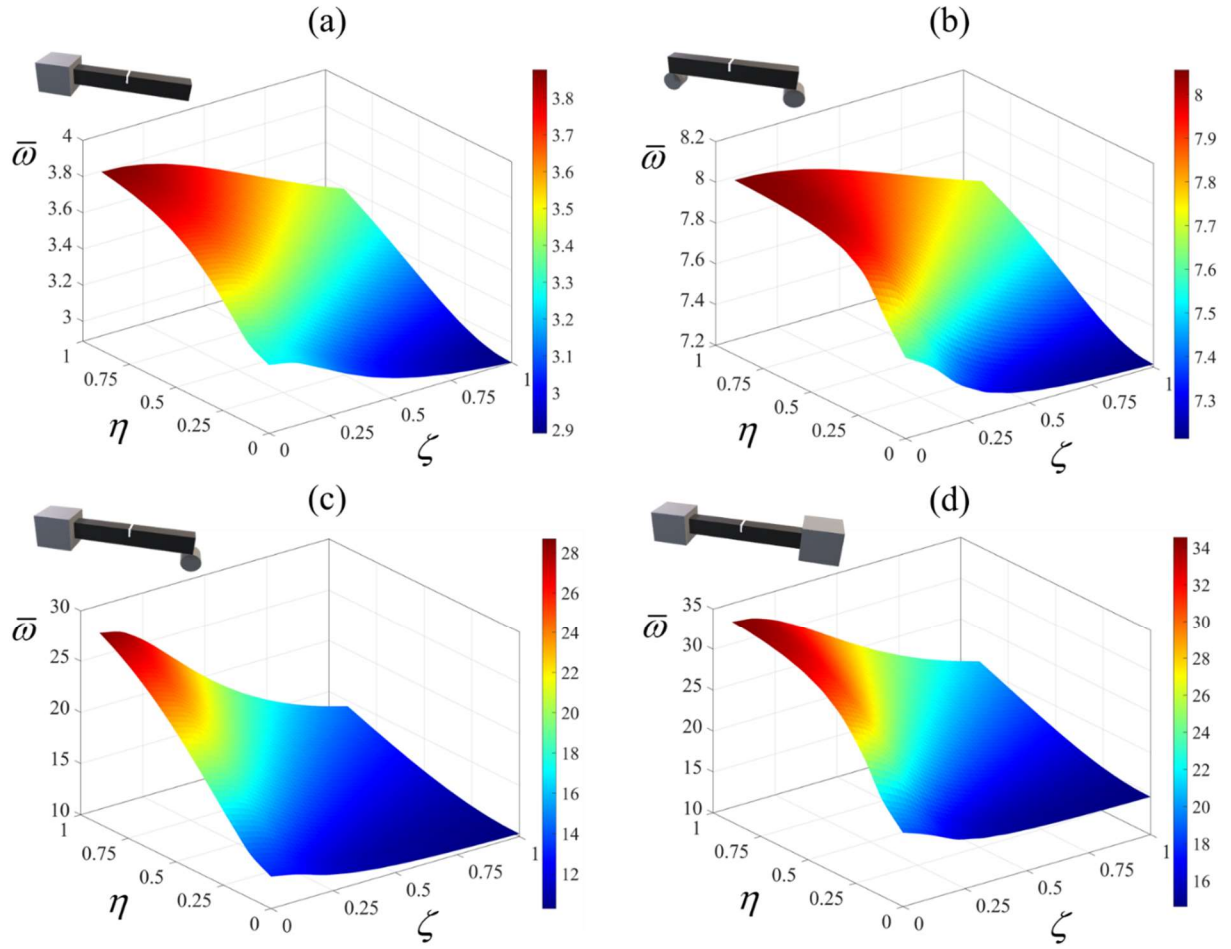

Fig. 4 Fundamental natural frequencies of the (a) clamped-free, (b) pinned-pinned, (c) clamped-pinned, and (d) clamped-clamped small-scale beam with $\bar{h}=0.1$ and one crack with a length of $a/h=0.5$ located at $\bar{x}_1=0.5$. The mixture parameter is set equal to 0.5 and results are presented on varying the stress and strain gradient parameters.

The ratios between fundamental natural frequencies of cracked and crack-free small-scale beams are examined for various boundary conditions in Fig. 5. The beams have a thickness-to-length ratio of 0.1 and one crack at the mid-span. The mixture parameter is fixed at 0.5, and the results are illustrated while changing the stress and strain gradient parameters for two different crack lengths.

Two main trends are evident from the results presented in Fig. 5. Firstly, the impact of the crack on the natural frequency depends on the stress and strain gradient parameters. Specifically, this effect is more pronounced when the stress and strain gradient parameters are lower and higher, respectively. Secondly, the influence of the stress and strain gradients on the frequency ratio intensifies with longer cracks. For instance, increasing the strain gradient parameter from 0 to 0.9, while the stress gradient parameter is fixed at 0.4, reduces the frequency ratio of the clamped-clamped beam by 15% and 54% for crack lengths of 0.25 and 0.5, respectively.

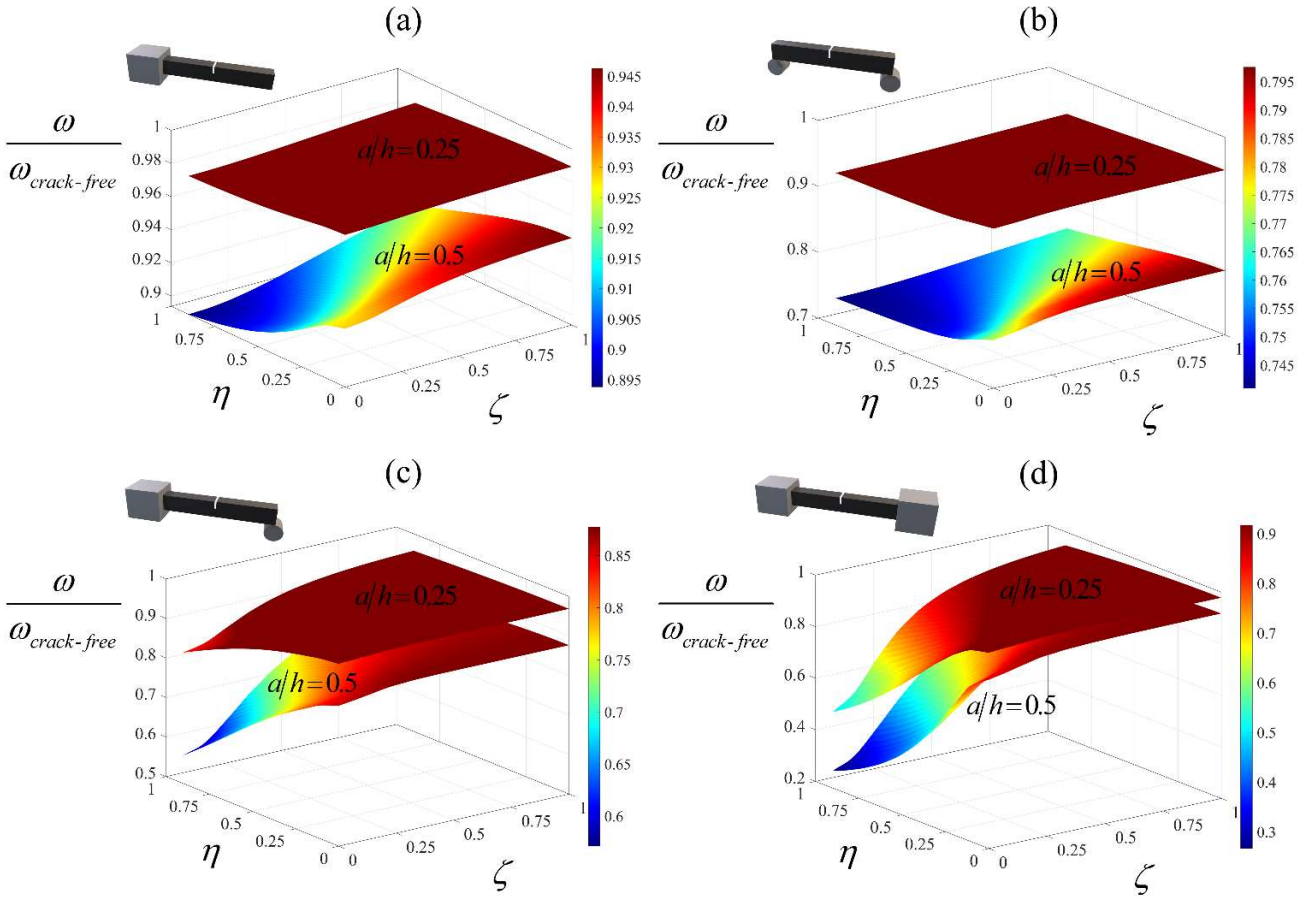

Fig. 5 Ratios between the fundamental natural frequencies of cracked and crack-free (a) clamped-free, (b) pinned-pinned, (c) clamped-pinned, and (d) clamped-clamped small-scale beam with $\bar{h} = 0.1$ and one crack

located at $\bar{x}_1 = 0.5$. The mixture parameter is set equal to 0.5 and results are presented on varying the stress and strain gradient parameters for two crack lengths.

The impact of crack length and location on the fundamental natural frequencies of small-scale beams with various boundary conditions is illustrated in Fig. 6. The results refer to small-scale beams with $\bar{h} = 0.1$, $\zeta = 0.4$, $\eta = \alpha = 0.5$. As anticipated, longer cracks consistently decrease the frequencies. However, the influence of crack location on the frequencies is more intricate. Specifically, when the crack is located at cross-sections experiencing higher bending moments, its effect is more pronounced. For instance, in a clamped-free beam, the frequency reduction is more pronounced when the crack is located closer to the fixed end. Conversely, when the crack is near the free end, even long cracks have minimal effects on the frequency. Moreover, the crack exerts its maximum influence on the frequency of pinned-pinned and clamped-clamped beams when positioned at the mid-span, where the bending moment is maximized. However, in a clamped-clamped beam, if the crack is located around 0.25 or 0.75, where the bending moment is negligible, its effect is minimized. The dependence of frequency on crack length and location, as illustrated in Fig. 6, aligns with observations made by other researchers who have applied various non-classical continuum mechanics-based theories to the same problem (e.g., [35]).

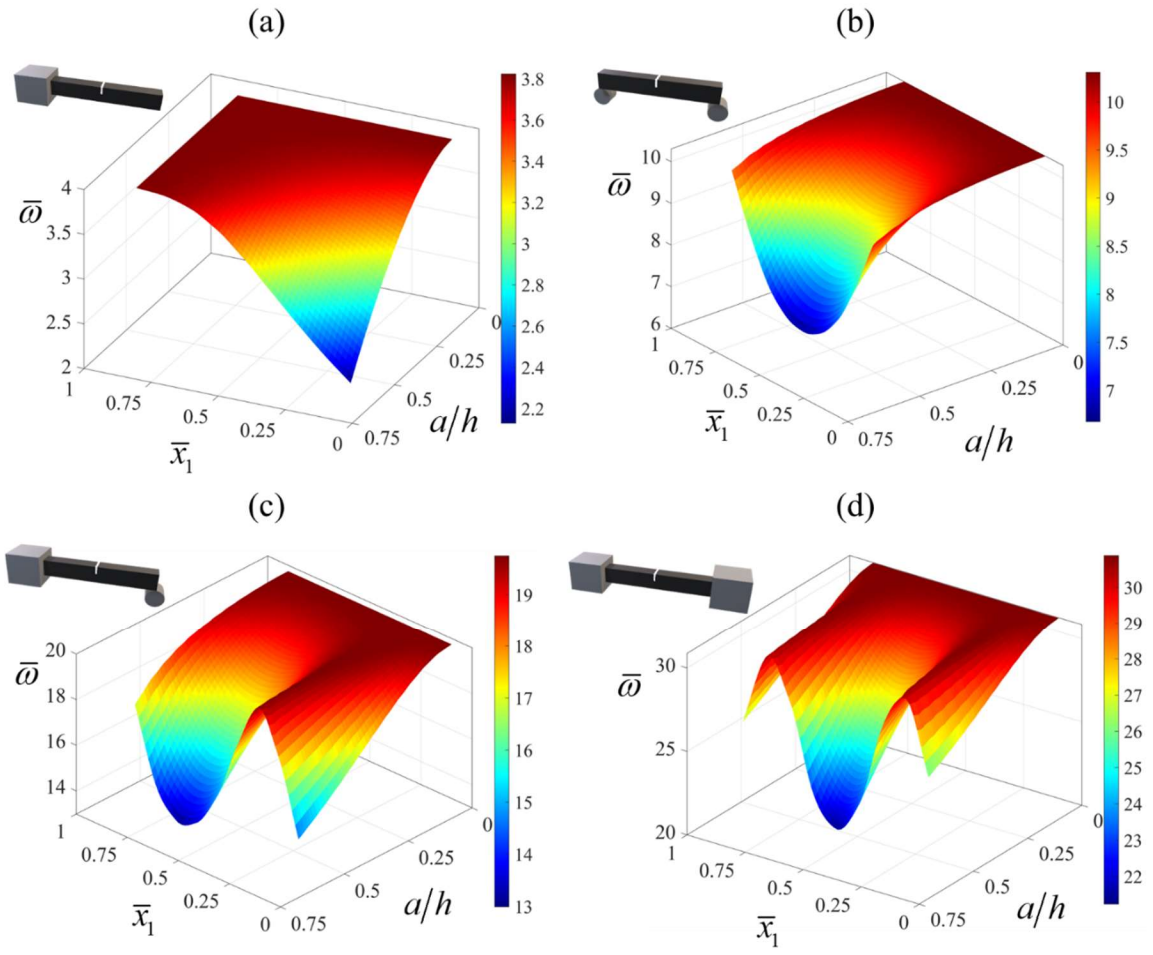

Fig. 6 Fundamental natural frequencies of the (a) clamped-free, (b) pinned-pinned, (c) clamped-pinned, and (d) clamped-clamped small-scale beam with $\bar{h}=0.1$, $\zeta=0.4$, $\eta=\alpha=0.5$. The results are presented for the small-scale beams with one crack varying its length and location.

As mentioned earlier, the effect of the crack on the natural frequencies is highly dependent on its location. This dependence is well described by the following statement: the closer the crack is to cross-sections with higher bending moments, the stronger its effect on the frequencies. Therefore, it is expected that the effect of crack location on natural frequencies differs for various modes of vibration. This is demonstrated in Fig. 7, where the natural frequencies of the first four vibration modes of a clamped-clamped small-scale beam with $\bar{h}=0.1$, $\zeta=0.4$, $\eta=\alpha=0.5$ are depicted. Results are presented by varying the crack length and location. When the crack is positioned at the mid-span, its effect on the first

natural frequency is maximized. However, the impact of a mid-span crack on the second frequency is negligible due to the vanishing bending moment at the mid-span during the second mode of vibration. Conversely, while cracks at 0.25 and 0.75 do not significantly affect the first frequency, they result in a notable reduction in the second frequency. Note that the frequencies always decrease with increasing crack length, regardless of the mode of vibration.

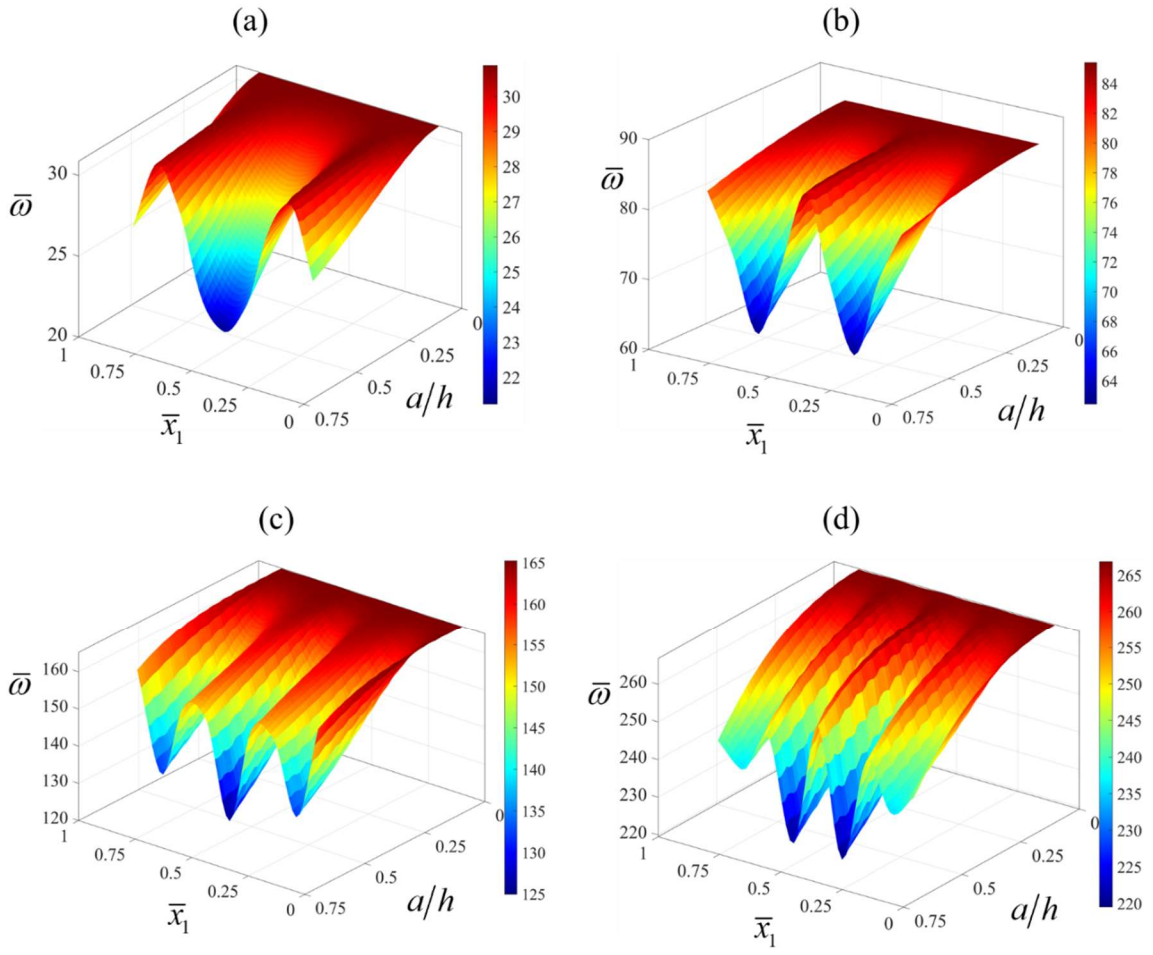

Fig. 7 Frequencies of the (a) first, (b) second, (c) third, and (d) fourth mode of vibration of a clamped-clamped small-scale beam with $\bar{h}=0.1$, $\zeta=0.4$, $\eta=\alpha=0.5$. The results are presented for the small-scale beams with one crack varying its length and location.

The effect of crack length and location also highly depends on the values of the gradient and mixture parameters. Results in Fig. 8 refer to the fundamental natural frequencies of clamped-clamped small-

scale beams with $\bar{h}=0.1$. In Fig. 8(a), the strain gradient and mixture parameters are held constant at $\eta=0.5$ and $\alpha=0$, while frequencies are presented by varying the crack length and location for three different values of the stress gradient parameter: 0, 0.3, and 0.6. The impact of crack length and location on the frequency is more pronounced when the small-scale beam is stiffer, particularly when the stress gradient parameter tends to zero. The same observation is also made in Fig. 8(b) and (c): the stiffer the beam, the greater the effect of crack length and location on the frequency. Specifically, the frequencies of small-scale beams with higher values of the strain gradient and mixture parameters are more sensitive to the presence of the crack.

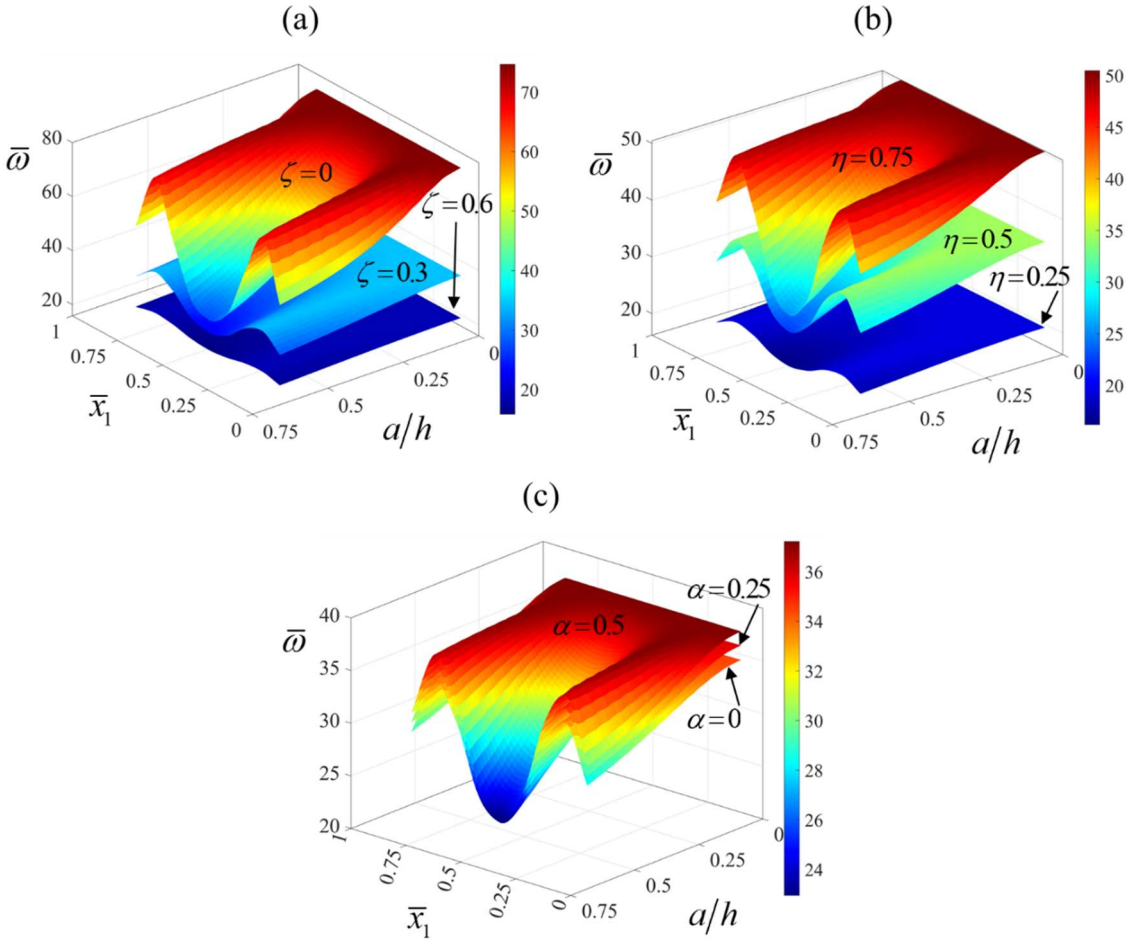

Fig. 8 Fundamental natural frequencies of the clamped-clamped small-scale beams with $\bar{h} = 0.1$. The results are presented for the cases with one crack on varying its length and location for (a) $\eta = 0.5$ and $\alpha = 0$, (b) $\zeta = 0.3$ and $\alpha = 0$, and (c) $\zeta = 0.3$ and $\eta = 0.5$.

3.3. Two Cracks

Application of the formulated model to small-scale beams with multiple cracks is straightforward. Here, small-scale beams with two cracks, $\bar{h} = 0.1$, $\zeta = \eta = 0.3$, and $\alpha = 0.5$, are studied. Four different boundary conditions are considered, and the fundamental natural frequencies are presented in Fig. 9, varying lengths of the first and second cracks symmetrically located about the mid-span, at $\bar{x}_1 = 0.35$ and $\bar{x}_2 = 0.65$. The effect of the second crack on the natural frequency of the clamped-free small-scale beam in Fig. 9(a) is weakened by the presence of the first crack, positioned closer to the fixed end with a higher bending moment. Similarly, the effect of the first crack located at $\bar{x}_1 = 0.35$ on the natural frequency of the clamped-pinned beam is shielded by the presence of the second crack. However, the effects of both cracks, which are symmetrically located about the mid-span, on the natural frequencies of the pinned-pinned and clamped-clamped beams are the same.

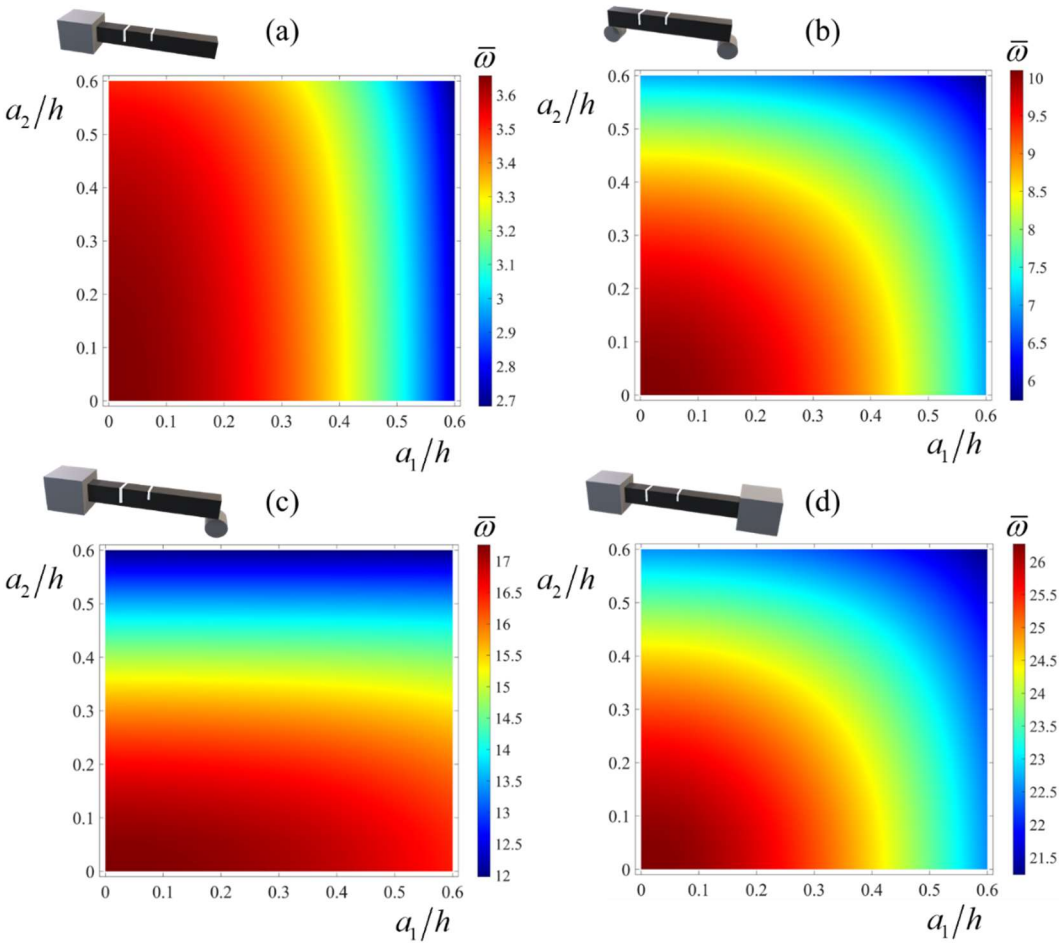

Fig. 9 Fundamental natural frequencies of the (a) clamped-free, (b) pinned-pinned, (c) clamped-pinned, and (d) clamped-clamped small-scale beam with $\bar{h}=0.1$, $\zeta=\eta=0.3$, and $\alpha=0.5$. The results are presented for the small-scale beams with two cracks located at $\bar{x}_1=0.35$ and $\bar{x}_2=0.65$ on varying crack lengths.

4. Conclusions

The impact of multiple edge cracks on the first and higher natural frequencies of small-scale beams is investigated. The mixture unified gradient elasticity theory is employed to capture size effects at small scales, incorporating stress and strain gradient characteristic lengths along with a mixture parameter into the formulation. Through rigorous mathematical treatment of the time-dependent variational functional, variationally consistent, and extra non-standard boundary and continuity conditions are derived. The natural frequencies are obtained by solving the eigenvalue problem constructed from the equilibrium equations associated with the Bernoulli-Euler beam model at different sections of the beam between the

edge cracks while imposing standard and extra non-standard boundary and continuity conditions. Continuity conditions at the cracked cross-sections are established by introducing linear elastic rotational and translational springs.

The accuracy of the formulated model is tested using two cases for which experimental and analytical results are available in the literature. Initially, it is demonstrated that the model accurately predicts experimental results regarding the frequencies of classical mesoscale cracked beams. Secondly, it is illustrated that the predictions of the model align with those of crack-free mixture unified gradient elastic beams as the crack length approaches zero. Subsequently, the model is employed to explore the impact of gradient and mixture parameters in addition to the crack length and location on the first and higher frequencies of nano-sized beams with various kinematic constraints. It is realized that the stress gradient characteristic parameter induces a softening effect, leading to reduced frequencies of small-scale cracked beams. Conversely, the strain gradient characteristic and mixture parameters contribute to a stiffening effect, resulting in increased frequencies. The influence of gradient parameters on the frequency ratio amplifies with longer cracks. Moreover, it is confirmed that frequencies consistently decrease with increasing crack length. The effect of crack length and location on natural frequency varies according to the prescribed values of stress and strain gradient parameters. Notably, this influence is more pronounced with lower stress gradient parameters and higher strain gradient parameters. The insights gained from the present study have potential implications for innovative design and damage detection in small-scale beams.

Funding

Hossein Darban gratefully acknowledges the financial support provided by the National Science Centre (NCN) in Poland through the grant agreement No: UMO-2022/47/D/ST8/01348.

Statements and Declarations

The authors declare that they have no known competing financial interests or personal relationships that could have appeared to influence the work reported in this paper.

Appendix A

Regarding mesoscale beams, there exists ample literature supporting the adoption of the simplified spring model in Eq. (2) for dynamic analyses of cracked beams. For instance, by utilizing the internal and external potential energies associated with the crack to establish the energy release rate as the negative derivative of the total potential energy concerning crack length, and establishing the connection between the energy release rate and the stress intensity factors, the crack compliances can be expressed in terms of the stress intensity factors and, consequently, directly in terms of the crack lengths [39, 40]. The crack compliances are determined in [40] for a rectangular mesoscale beam with an edge crack under plane stress conditions:

$$c_i^M = 12Ch\int_0^{\beta_i} F_M^2\left(\beta_i\right)d\beta_i \qquad \text{for } 0 \le \beta_i \le 0.6$$

$$F_M\left(\beta_i\right) = \sqrt{\tan\frac{\pi\beta_i}{2}}\,\frac{0.923 + 0.199\left[1-\sin\frac{\pi\beta_i}{2}\right]^4}{\cos\frac{\pi\beta_i}{2}} \tag{A.1}$$

$$c_i^M = 2.65335Ch\int_0^{\beta_i}\frac{1}{\left(1-\beta_i\right)^3}d\beta_i \qquad \text{for } 0.6 < \beta_i < 1$$

and

$$c_i^V = \frac{1}{6} C h^3 \int_0^{\beta_i} \frac{1}{1-\beta_i} F_V^2(\beta_i)\, d\beta_i \qquad \text{for } 0 \le \beta_i < 1$$

$$F_V(\beta_i) = 1.993\beta_i + 4.513\beta_i^2 - 9.516\beta_i^3 + 4.482\beta_i^4 \tag{A.2}$$

where $\beta_i = a_i/h$ is the relative length of the *i*-th crack with respect to the nanobeam thickness, and $C = 1/(EI)$. Furthermore, natural frequencies of mesoscale cracked beams obtained using the elastic spring model have shown excellent agreement with experimental findings, even for higher vibration modes [40]. Therefore, it is reasonable to assert that conducting vibration analysis on mesoscale cracked beams using the conditions outlined in Eqs. (2), (A.1), and (A.2) yields accurate results.

The closed-form expressions for the crack compliances in Eqs. (A.1) and (A.2) are derived based on local fracture mechanics, and therefore, may not necessarily be applicable at small scales. Particularly at the atomistic level, van der Waals forces between atoms positioned at the surfaces of the crack tend to induce closure, potentially affecting the kinematic compatibility conditions. Nonetheless, these equations are applied in this study to define the crack compliances in terms of crack length. Even if Eqs. (A.1) and (A.2) are required to be improved, the conclusions of the present study remain valid.

It is also assumed that the cracks do not propagate during vibration and are sufficiently distant from each other, ensuring that their local crack tip stress fields remain undisturbed. Consequently, the model does not account for crack interactions that may result in stress amplification or shielding. However, assuming non-interacting cracks enables the definition of the local compliance of each crack based on its length using Eqs. (A.1) and (A.2), and allows for investigating the impact of a system of *n* cracks on natural frequencies.

Data Availability

Data will be made available on request.

References

1. Lavrik, N. V., Sepaniak, M. J., & Datskos, P. G. (2004). Cantilever transducers as a platform for chemical and biological sensors. *Review of Scientific Instruments*, *75*(7), 2229–2253. https://doi.org/10.1063/1.1763252
2. Tang, C., & Alici, G. (2011). Evaluation of length-scale effects for mechanical behaviour of micro- and nanocantilevers: II. Experimental verification of deflection models using atomic force microscopy. *Journal of Physics D: Applied Physics*, *44*(33), 335502. https://doi.org/10.1088/0022-3727/44/33/335502
3. Lam, D. C. C., Yang, F., Chong, A. C. M., Wang, J., & Tong, P. (2003). Experiments and theory in strain gradient elasticity. *Journal of the Mechanics and Physics of Solids*, *51*(8), 1477–1508. https://doi.org/10.1016/S0022-5096(03)00053-X
4. Fernández-Sáez, J., Zaera, R., Loya, J. A., & Reddy, J. N. (2016). Bending of Euler–Bernoulli beams using Eringen's integral formulation: A paradox resolved. *International Journal of Engineering Science*, *99*, 107–116. https://doi.org/10.1016/j.ijengsci.2015.10.013
5. Aria, A. I., Friswell, M. I., & Rabczuk, T. (2019). Thermal vibration analysis of cracked nanobeams embedded in an elastic matrix using finite element analysis. *Composite Structures*, *212*, 118–128. https://doi.org/10.1016/j.compstruct.2019.01.040
6. Loya, J., López-Puente, J., Zaera, R., & Fernández-Sáez, J. (2009). Free transverse vibrations of cracked nanobeams using a nonlocal elasticity model. *Journal of Applied Physics*, *105*(4), 044309. https://doi.org/10.1063/1.3068370
7. Eremeyev, V. A., Cazzani, A., & dell'Isola, F. (2021). On nonlinear dilatational strain gradient elasticity. *Continuum Mechanics and Thermodynamics*, *33*(4), 1429–1463. https://doi.org/10.1007/s00161-021-00993-6
8. Barretta, R., Luciano, R., Marotti de Sciarra, F., & Vaccaro, M. S. (2024). On torsion of FG elastic nanobeams on nonlocal foundations. *Composite Structures*, *340*, 118146. https://doi.org/10.1016/j.compstruct.2024.118146
9. Darban, H., Luciano, R., Caporale, A., & Basista, M. (2022). Modeling of buckling of nanobeams embedded in elastic medium by local-nonlocal stress-driven gradient elasticity theory. *Composite Structures*, *297*, 115907. https://doi.org/10.1016/j.compstruct.2022.115907
10. Eremeyev, V. A., & Lazar, M. (2022). Strong ellipticity within the Toupin–Mindlin first strain gradient elasticity theory. *Mechanics Research Communications*, *124*, 103944. https://doi.org/10.1016/j.mechrescom.2022.103944
11. Barretta, R., Feo, L., Luciano, R., & Marotti de Sciarra, F. (2016). An Eringen-like model for Timoshenko nanobeams. *Composite Structures*, *139*, 104–110. https://doi.org/10.1016/j.compstruct.2015.11.048
12. Hache, F., Challamel, N., & Elishakoff, I. (2019). Asymptotic derivation of nonlocal plate models from three-dimensional stress gradient elasticity. *Continuum Mechanics and Thermodynamics*, *31*(1), 47–70. https://doi.org/10.1007/s00161-018-0622-1
13. Barretta, R., Čanađija, M., & de Sciarra, F. M. (2019). Nonlocal integral thermoelasticity: A thermodynamic framework for functionally graded beams. *Composite Structures*, *225*, 111104. https://doi.org/10.1016/j.compstruct.2019.111104
14. Hache, F., Challamel, N., & Elishakoff, I. (2019). Asymptotic derivation of nonlocal beam models from two-dimensional nonlocal elasticity. *Mathematics and Mechanics of Solids*, *24*(8), 2425–2443. https://doi.org/10.1177/1081286518756947

15. Darban, H., Luciano, R., & Basista, M. (2023). Calibration of the length scale parameter for the stress-driven nonlocal elasticity model from quasi-static and dynamic experiments. *Mechanics of Advanced Materials and Structures*, *30*(17), 3518–3524. https://doi.org/10.1080/15376494.2022.2077488
16. Zhang, P., Schiavone, P., Qing, H., & Li, Q. (2025). Stress-driven nonlocal integral model with discontinuities for transverse vibration of multi-cracked non-uniform Timoshenko beams with general boundary conditions. *Composite Structures*, *353*, 118712. https://doi.org/10.1016/j.compstruct.2024.118712
17. Barretta, R., Fazelzadeh, S. A., Feo, L., Ghavanloo, E., & Luciano, R. (2018). Nonlocal inflected nano-beams: A stress-driven approach of bi-Helmholtz type. *Composite Structures*, *200*, 239–245. https://doi.org/10.1016/j.compstruct.2018.04.072
18. Saimi, A., Bensaid, I., & Civalek, Ö. (2023). A study on the crack presence effect on dynamical behaviour of bi-directional compositionally imperfect material graded micro beams. *Composite Structures*, *316*, 117032. https://doi.org/10.1016/j.compstruct.2023.117032
19. Chen, Y., Dorgan, B. L., Jr., McIlroy, D. N., & Eric Aston, D. (2006). On the importance of boundary conditions on nanomechanical bending behavior and elastic modulus determination of silver nanowires. *Journal of Applied Physics*, *100*(10), 104301. https://doi.org/10.1063/1.2382265
20. Li, X., Ono, T., Wang, Y., & Esashi, M. (2003). Ultrathin single-crystalline-silicon cantilever resonators: Fabrication technology and significant specimen size effect on Young's modulus. *Applied Physics Letters*, *83*(15), 3081–3083. https://doi.org/10.1063/1.1618369
21. Gupta, A. K., Nair, P. R., Akin, D., Ladisch, M. R., Broyles, S., Alam, M. A., & Bashir, R. (2006). Anomalous resonance in a nanomechanical biosensor. *Proceedings of the National Academy of Sciences*, *103*(36), 13362–13367. https://doi.org/10.1073/pnas.0602022103
22. Faghidian, S. A., & Elishakoff, I. (2022). Wave Propagation in Timoshenko–Ehrenfest Nanobeam: A Mixture Unified Gradient Theory. *Journal of Vibration and Acoustics*, *144*(061005). https://doi.org/10.1115/1.4055805
23. Lim, C. W., Zhang, G., & Reddy, J. N. (2015). A higher-order nonlocal elasticity and strain gradient theory and its applications in wave propagation. *Journal of the Mechanics and Physics of Solids*, *78*, 298–313. https://doi.org/10.1016/j.jmps.2015.02.001
24. Faghidian, S. A., Żur, K. K., & Pan, E. (2023). Stationary variational principle of mixture unified gradient elasticity. *International Journal of Engineering Science*, *182*, 103786. https://doi.org/10.1016/j.ijengsci.2022.103786
25. Faghidian, S. A., & Tounsi, A. (2022). Dynamic Characteristics of Mixture Unified Gradient Elastic Nanobeams. *Facta Universitatis, Series: Mechanical Engineering*, *20*(3), 539–552. https://doi.org/10.22190/FUME220703035F
26. Żur, K. K., & Faghidian, S. A. (Eds.). (2024). *Nanomechanics of Structures and Materials: Modeling and Analysis*. Elsevier. https://doi.org/10.101 /C2023-0-00141-8
27. Faghidian, S. A., & Darban, H. (2024). Non-standard interface conditions in flexure of mixture unified gradient Nanobeams. *International Journal of Engineering Science*, *204*, 104127. https://doi.org/10.1016/j.ijengsci.2024.104127
28. Faghidian, S. A., & Elishakoff, I. (2023). The tale of shear coefficients in Timoshenko–Ehrenfest beam theory: 130 years of progress. *Meccanica*, *58*(1), 97–108. https://doi.org/10.1007/s11012-022-01618-1
29. Chati, M., Rand, R., & Mukherjee, S. (1997). Modal Analysis of a Cracked Beam. *Journal of Sound and Vibration*, *207*(2), 249–270. https://doi.org/10.1006/jsvi.1997.1099
30. Fernández-sáez, J., & Navarro, C. (2002). Fundamental Frequency of Cracked Beams in Bending Vibrations: An Analytical Approach. *Journal of Sound and Vibration*, *256*(1), 17–31. https://doi.org/10.1006/jsvi.2001.4197

31. Wu, X.-W., Zhu, L.-F., Wu, Z.-M., & Ke, L.-L. (2022). Vibrational power flow analysis of Timoshenko microbeams with a crack. *Composite Structures*, *289*, 115483. https://doi.org/10.1016/j.compstruct.2022.115483
32. Morassi, A., Fernández-Sáez, J., Zaera, R., & Loya, J. A. (2017). Resonator-based detection in nanorods. *Mechanical Systems and Signal Processing*, *93*, 645–660. https://doi.org/10.1016/j.ymssp.2017.02.019
33. Dilena, M., Dell'Oste, M. F., Fernández-Sáez, J., Morassi, A., & Zaera, R. (2019). Identification of general added mass distribution in nanorods from two-spectra finite data. *Mechanical Systems and Signal Processing*, *134*, 106286. https://doi.org/10.1016/j.ymssp.2019.106286
34. Fernández-Sáez, J., Morassi, A., Rubio, L., & Zaera, R. (2019). Transverse free vibration of resonant nanoplate mass sensors: Identification of an attached point mass. *International Journal of Mechanical Sciences*, *150*, 217–225. https://doi.org/10.1016/j.ijmecsci.2018.09.055
35. Darban, H., Luciano, R., & Basista, M. (2022). Free transverse vibrations of nanobeams with multiple cracks. *International Journal of Engineering Science*, *177*, 103703. https://doi.org/10.1016/j.ijengsci.2022.103703
36. Ali Faghidian, S. (2017). Analytical Inverse Solution of Eigenstrains and Residual Fields in Autofrettaged Thick-Walled Tubes. *Journal of Pressure Vessel Technology*, *139*(031205). https://doi.org/10.1115/1.4034675
37. Ali Faghidian, S. (2017). Analytical Approach for Inverse Reconstruction of Eigenstrains and Residual Stresses in Autofrettaged Spherical Pressure Vessels. *Journal of Pressure Vessel Technology*, *139*(041202). https://doi.org/10.1115/1.4035980
38. Gudmundson, P. (1982). Eigenfrequency changes of structures due to cracks, notches or other geometrical changes. *Journal of the Mechanics and Physics of Solids*, *30*(5), 339–353. https://doi.org/10.1016/0022-5096(82)90004-7
39. Freund, L. B., & Herrmann, G. (1976). Dynamic Fracture of a Beam or Plate in Plane Bending. *Journal of Applied Mechanics*, *43*(1), 112–116. https://doi.org/10.1115/1.3423760
40. Yokoyama, T., & Chen, M.-C. (1998). Vibration analysis of edge-cracked beams using a line-spring model. *Engineering Fracture Mechanics*, *59*(3), 403–409. https://doi.org/10.1016/S0013-7944(97)80283-4